Structure
Article

Structural and Functional Characterization of Alternative Transmembrane Domain Conformations in VEGF Receptor 2 Activation

Sandro Manni,[1,6] Konstantin S. Mineev,[2,6] Dinara Usmanova,[2,3] Ekaterina N. Lyukmanova,[2] Mikhail A. Shulepko,[2,4] Mikhail P. Kirpichnikov,[2,4] Jonas Winter,[1] Milos Matkovic,[1] Xavier Deupi,[1,5] Alexander S. Arseniev,[2,3,7] and Kurt Ballmer-Hofer[1,7,*]

[1]Paul Scherrer Institute, Biomolecular Research, 5232 Villigen PSI, Switzerland
[2]Shemyakin-Ovchinnikov Institute of Bioorganic Chemistry RAS, Miklukho-Maklaya Street 16/10, Moscow 117997, Russian Federation
[3]Moscow Institute of Physics and Technology, Institutskiy Pereulok 9, Dolgoprudny, Moscow Region 141700, Russian Federation
[4]Lomonosov Moscow State University, Leninskie Gori 1, Moscow 119234, Russian Federation
[5]Paul Scherrer Institute, Condensed Matter Theory Group, 5232 Villigen PSI, Switzerland
[6]Co-first author
[7]Co-senior author
*Correspondence: kurt.ballmer@psi.ch
http://dx.doi.org/10.1016/j.str.2014.05.010

SUMMARY

Transmembrane signaling by receptor tyrosine kinases (RTKs) entails ligand-mediated dimerization and structural rearrangement of the extracellular domains. RTK activation also depends on the specific orientation of the transmembrane domain (TMD) helices, as suggested by pathogenic, constitutively active RTK mutants. Such mutant TMDs carry polar amino acids promoting stable transmembrane helix dimerization, which is essential for kinase activation. We investigated the effect of polar amino acids introduced into the TMD of vascular endothelial growth factor receptor 2, regulating blood vessel homeostasis. Two mutants showed constitutive kinase activity, suggesting that precise TMD orientation is mandatory for kinase activation. Nuclear magnetic resonance spectroscopy revealed that TMD helices in activated constructs were rotated by 180° relative to the interface of the wild-type conformation, confirming that ligand-mediated receptor activation indeed results from transmembrane helix rearrangement. A molecular dynamics simulation confirmed the transmembrane helix arrangement of wild-type and mutant TMDs revealed by nuclear magnetic resonance spectroscopy.

INTRODUCTION

The human genome encodes 58 receptor tyrosine kinases (RTKs) that regulate cellular activities such as growth, migration, differentiation, and survival. RTKs exist either as preformed dimers or are dimerized upon ligand binding. In both cases, ligand binding leads to conformational changes in the receptor extracellular domain (ECD), as for instance shown for type I, III, IV, and V RTKs (Schlessinger, 2003; Lemmon and Ferguson, 2007). The structural changes in the ECD of receptor dimers subsequently instigate transmembrane signaling by reorienting the intracellular kinase domains.

We studied vascular endothelial growth factor receptors (VEGFRs) that regulate blood and lymphatic vessel development and homeostasis. Deregulated VEGFR signaling, resulting for instance from overexpression of VEGF or VEGF receptors, causes many pathologies (Koch et al., 2011), and mutation of VEGFR-2 has been shown to be associated with juvenile hemangioma (Jinnin et al., 2008). In addition to extensive biochemical evidence, structural analysis by single particle electron microscopy (Ruch et al., 2007), small angle X-ray solution scattering (Kisko et al., 2011), and X-ray crystallography (Leppänen et al., 2013; Brozzo et al., 2012; Leppänen et al., 2010) showed that ligand binding to VEGFR-2 promotes receptor dimerization. These studies also show that structural rearrangements in membrane-proximal VEGFR-2 ECD subdomains allosterically regulate receptor activation (Hyde et al., 2012). High-resolution structural information is also available for other ligand-RTK complexes (Yuzawa et al., 2007; Stauber et al., 2000; Pellegrini et al., 2000; Plotnikov et al., 1999; Liu et al., 2007; Barton et al., 2006; Ogiso et al., 2002), and X-ray crystallography of soluble kinase domain constructs revealed essential details regarding the mechanism of RTK activation (Zhang et al., 2006; Walter et al., 2007; Schubert et al., 2007). The kinase domains of epidermal growth factor receptor (EGFR) and fibroblast growth factor receptor (FGFR), for instance, have been shown to form asymmetric dimers stabilized by interactions between the juxtamembrane domain and the upper and lower lobes of the kinase (Endres et al., 2013; Zhang et al., 2006; Bae et al., 2010; Jura et al., 2009). These asymmetric dimers represent the active state of these receptor kinases and have also been confirmed for the full-length EGFR (Mi et al., 2011) and FGFR (Opatowsky et al., 2014) by single particle electron microscopy.

The importance of dimerization in RTK activation is, therefore, well documented, and aberrant signaling because of mutations that lead to ligand-independent dimer formation are the cause of many diseases. For example, ligand-independent dimerization of mutant Neu receptors, an EGFR homolog, promotes

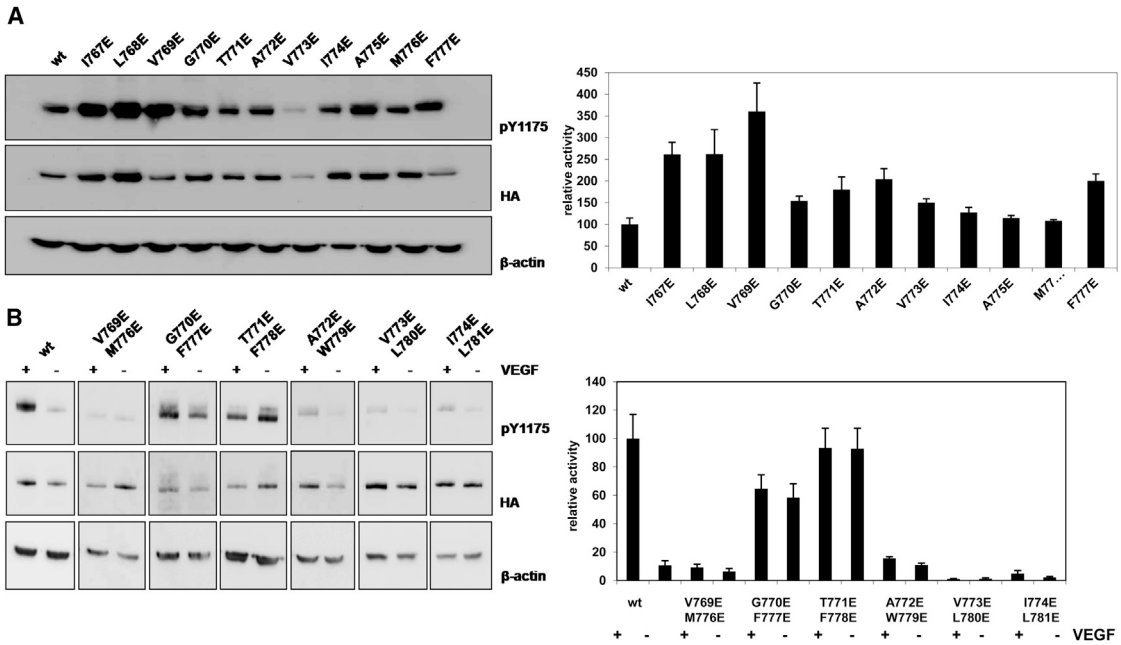

Figure 1. Kinase Activities of Single Glutamic Acid TMD Mutants of ΔECD-VEGFR-2 and Double Glutamic Acid TMD Mutants of Full-Length VEGFR-2 Constructs Determined by Analysis of Y1175 Phosphorylation on Western Blots

(A and B) Graphs show the quantification of three independent experiments with SD. The y axis represents relative activity. Figure S1 shows a summary of the constructs used in this analysis.

tumorigenesis (Bargmann and Weinberg, 1988; Smith et al., 1996). Such Neu mutants carried a valine-to-glutamic acid substitution in the transmembrane domain (TMD) that led to ligand-independent receptor activation (Smith et al., 1996; Gullick et al., 1992). Similarly, mutation of the TMD of FGFR3 causes developmental disorders such as bone malformation or oncogenic transformation (Kelleher et al., 2013; Webster and Donoghue, 1996). Based on these results, Bell et al. (2000) engineered constitutively dimerized Neu and platelet-derived growth factor receptor (PDGFR) constructs by replacing the TMD with a hydrophobic helix comprising 25 valine residues interrupted by two polar amino acids, such as glutamic acid, spaced seven amino acids apart and, therefore, located on the same face of the helix (Bell et al., 2000). These mutations gave rise to highly stable dimers that were either active or inactive, depending on where the polar residues were located in the TMD. We applied this concept to VEGFR-2 and found that only one distinct conformation rendered the receptor constitutively active, showing that receptor dimerization is necessary, but not sufficient, for VEGFR-2 activation (Dosch and Ballmer-Hofer, 2010).

Here we applied scanning mutagenesis to the WT TMD and correlated the activity of constructs carrying glutamic acid residues in specific positions with their structure determined by nuclear magnetic resonance (NMR) spectroscopy. Molecular dynamics (MD) simulations further support the structural and dynamic interpretation of the NMR data. Our data show that introducing two polar amino acids in distinct positions of the TMD reorients transmembrane helices and leads to stable dimer formation. Therefore, we infer that the transition between the inactive and the active dimeric state of VEGFR-2 implicates alternative dimeric TMD conformations.

RESULTS

Construction and Analysis of Constitutively Dimerized VEGFR-2 TMD Variants

To investigate the role of the TMD in VEGFR-2 signaling, we generated constitutively dimerized, ECD-truncated and full-length receptor constructs. These constructs carried transmembrane helices with either one or two residues replaced by glutamic acid (for a summary scheme of all constructs, see Figures S1A and S1B available online). The ECD-deleted construct carrying glutamic acid in position 769 (V769E) exhibited the highest activity (Figure 1A, top panels), whereas the mutants I767E and L768E had a lower, but still increased activity compared with the WT TMD construct. The ECD-deleted WT TMD construct showed only 20%–30% of the activity of the activating mutants but was clearly more active than the full-length receptor in the absence of ligand, reaching about 50% of the activity of the ligand-stimulated, full-length receptor (Figure S2A). This shows, similar to other RTKs, that receptor dimerization and, thus, kinase activation is negatively regulated by the ECD (Dosch and Ballmer-Hofer, 2010).

In the full-length VEGFR-2, the V769E mutation was not activating, presumably because of steric constraints by the receptor ECD that prevent the proper alignment of the two helices in the membrane. As a matter of fact, none of the single mutant TMD constructs showed ligand-independent activity (Figure S3). Therefore, we generated double mutant TMD constructs carrying two glutamic acid residues spaced seven amino acids apart. In these constructs, the polar amino acids are predicted to face the same side of the TMD, giving rise to highly stable dimers. Figure 1B shows that the G770E/F777E and T771E/F778E

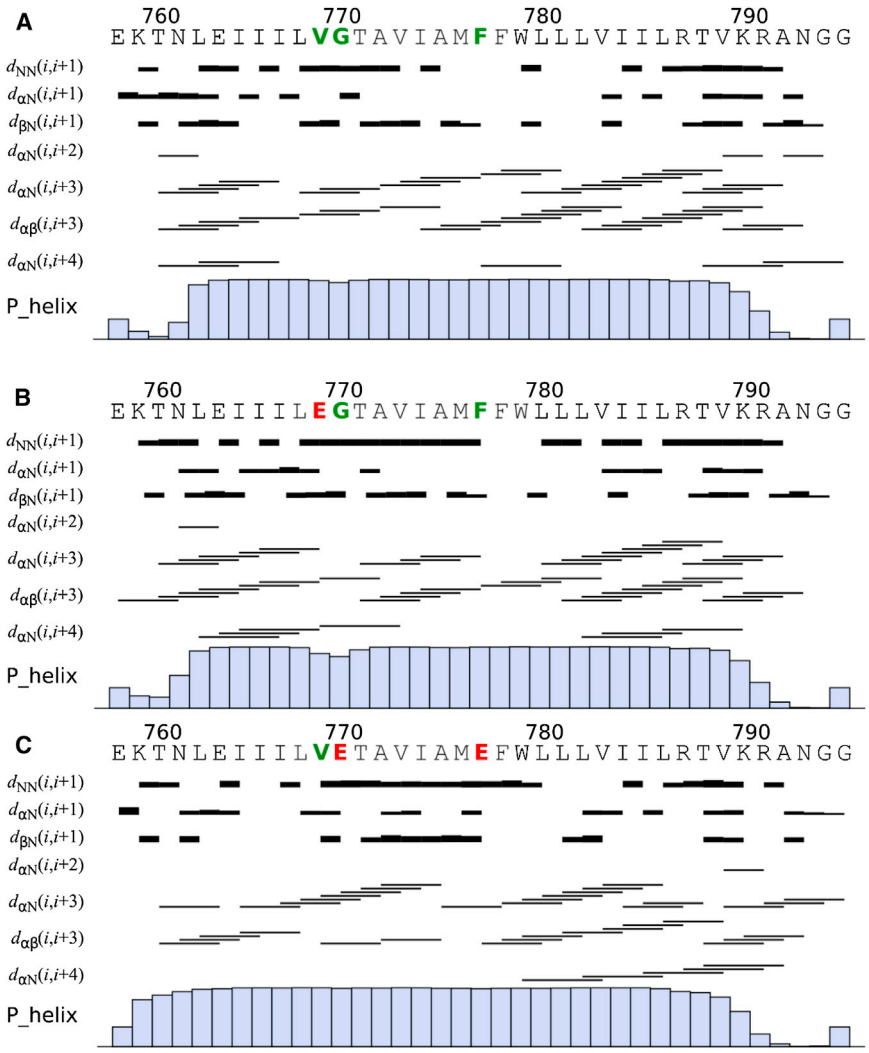

Figure 2. NMR Data and Secondary Structure of the Peptides VEGFR-2tm, VEGFR-2tm769, and VEGFR-2tm770/777

(A–C) Sequential and medium-range characteristic NOE-based distances (d_{XX}(i1,i2) are shown as horizontal lines. Line thickness is proportional to the intensity of the corresponding peak in the NOESY spectrum. Meaningless contacts, i.e., contacts that do not impose any restraints on the structure, were removed by the built-in algorithm in the CYANA software (Guentert, 2003). P_helix is the α helix propensity predicted by the TALOS+ (Shen et al., 2009) software on the basis of NMR chemical shifts.

mutants had high constitutive receptor activity, which was not increased further by ligand addition. To rule out improper intracellular trafficking of such constructs and, thus, inaccessibility to extracellular ligand, we compared the membrane localization of WT and mutant TMD receptors by immunofluorescence microscopy in transfected COS-7 cells. To further demonstrate membrane localization of these mutant receptors, the cells were cotransfected with a plasmid encoding a fluorescent membrane marker. We used an enhanced green fluorescent protein (EGFP) fusion protein of the pleckstrin homology (PH) domain of phospholipase δ that binds to phosphatidylinositol 4,5-bisphosphate. VEGFR-2 was labeled prior to fixation with an antibody recognizing the receptor ECD (Figure S2B). In agreement with our work published earlier, confocal microscopy clearly showed plasma membrane staining of both the eGFP-PH membrane marker and VEGFR-2 (Dosch and Ballmer-Hofer, 2010).

Taken together, our data show that replacement of a single residue in the TMD by a polar amino acid in either of three positions is sufficient for activation of ECD-truncated VEGFR-2, whereas mutation of two residues in either of two positions is required for activation of full-length receptors.

NMR Analysis and 3D Structure of WT and Mutant TMDs in DPC Micelles

To analyze the effect of the identified mutations on the structural and thermodynamic properties of TMD helix-helix interactions, we determined the structures and measured the free energies of dimerization for peptides representing WT (VEGFR-2tm) and the activating mutants VEGFR-2tm769 and VEGFR-2tm770/777. TMD peptides were produced in vitro and inserted into membrane-mimetic dodecylphosphocholine (DPC) micelles. NMR chemical shifts, nuclear Overhauser effect (NOE) connectivities, and NMR relaxation data revealed that the WT peptide forms a long α helix between residues 761 and 794 (Figure 2). VEGFR-2tm existed in two forms, with population states depending on the detergent-to-protein ratio (for details, see Supplemental Experimental Procedures). Dilution by detergent revealed that these states represented monomers and dimers, respectively. The monomer-dimer transition was very slow, in the range of seconds, with the free energy of dimerization equal to −2.1 ± 0.2 kilocalories (kcal)/mol (Figure 3A). The reported free energies were obtained as described by Mineev et al. (2014), using standard conditions corresponding to a micelle concentration of 1M. The free energy of dimerization of VEGFR-2tm was clearly lower than that observed for other RTKs, such as ErbB3 (−0.5 kcal/M), ErbB4 (−1.5 kcal/M), and FGFR3 (−1.4 kcal/M).

For the WT VEGFR-2tm peptide, we detected nine intermonomeric contacts by heteronuclei-filtered NOE spectroscopy (NOESY), which were used to calculate the 3D structure of TMD dimers. A summary of NMR data and statistics of the calculated structures is given in Table 1. The WT structure represents a symmetric, left-handed parallel dimer with an angle between helical axes of 25 ± 1° (Figure 5A). The interface of dimerization is long and encompasses almost the entire length of the TMD segment. The interaction between α helices is accomplished via a heptad repeat-like motif T^{761}xxE^{764}xx$I^{767}L^{768}$xxT^{771} A^{772}xxA^{775}xx$F^{778}W^{779}$x$L^{781}L^{782}$xxI^{785}xxxV^{789}. The association

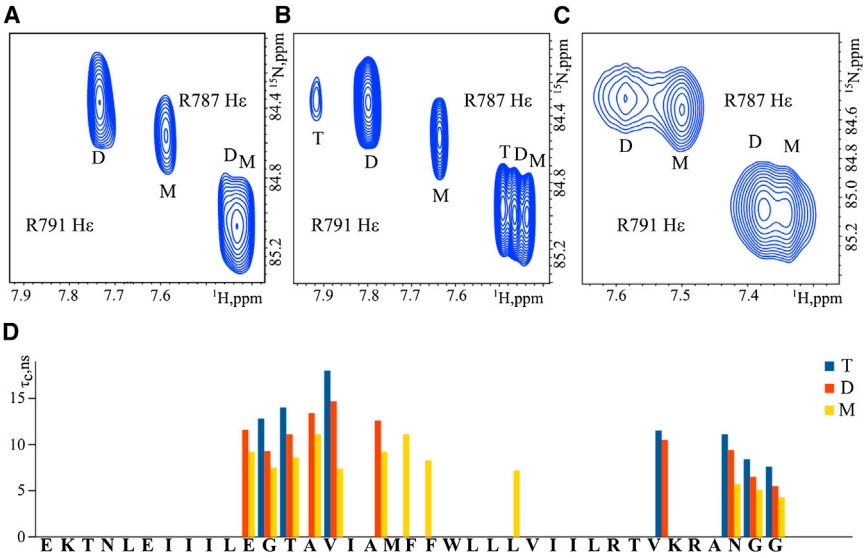

Figure 3. TROSY-HSQC Spectra of TMD Peptides

(A–C) Signals arising from interhelical Nε-H interactions between arginines 787 and 791 in $^{1}H,^{15}N$-TROSY-HSQC spectra of the peptides VEGFR-2tm (A), VEGFR-2tm769 (B), and VEGFR-2tm770/777 (C). Cross-peaks originating from different oligomeric states are assigned: M (monomer), D (dimer) and T (trimer). All spectra were acquired at lipid/protein ratios of 300:1 at 318 K and pH 4.5 on a Bruker AVANCE III 800-MHz spectrometer.

(D) NMR-derived correlation time for the rotational diffusion measured from cross-correlated relaxation rates of N-H groups of VEGFR-2tm769 for three oligomeric states: monomer (yellow bars), dimer (red bars), and trimer (blue bars).

of the VEGFR-2tm peptide is stabilized by stacking of the aromatic side chains of F778 and W779 and by van der Waals contacts between bulky side chains of hydrophobic residues. The observed VEGFR-2tm dimer conformation is similar to previously determined structures of dimeric TMDs of EphA2 (Bocharov et al., 2010), ErbB3 (Mineev et al., 2011), and FGFR3 (Bocharov et al., 2013).

We next studied the effect of the V769E substitution on the VEGFR-2 TMD structure. The VEGFR-2tm769 peptide was inserted into DPC micelles at pH 4.5. Under these conditions, the side chains of E764 and E769 were protonated (Figure S5). The NMR spectra of VEGFR-2tm769 were very similar to WT VEGFR-2tm, displaying multiple contacts between methyl groups in isoleucine, valine, and leucine residues to residual protons of the DPC methyl groups in ^{13}C-filtered NOESY (Figure 2). This shows that the peptide is in a "transmembrane" and not in a "surface-bound" orientation. The side chain of the transmembrane E769 was protonated under both experimental (pH 4.5) and physiological (pH 7.0) conditions (Figure S5). The secondary chemical shifts show that the α helix of VEGFR-2tm769 is present in the same section of the peptide as in the WT. Unlike the WT, the single mutant TMD formed three oligomeric states, characterized by different correlation times for rotational diffusion (Figures 4A and 4B; Figures S4A and S4B). The samples were gradually diluted to determine peptide oligomerization and to measure the effect of the valine-to-glutamic acid substitution on oligomerization propensity. Three models for the oligomerization equilibrium were tested: monomer-dimer1-dimer2, monomer-dimer-trimer, and monomer-dimer-tetramer. The trimerization model best fit the data obtained (Figures 3B and 3D; Figure S4B) with a free energy of the dimer (ΔG_{dim}) of -2.4 ± 0.2 kcal/mol and a free energy of the trimer (ΔG_{trim}) of -2.9 ± 0.2 kcal/mol. The change in the free energy of dimerization caused by the V769E mutation was insignificant, accounting for only 0.3 kcal/mol, which is within the experimental error. The population of the monomer, dimer, and trimer states depended on the peptide-to-detergent ratio. We were not able to calculate the dimer structure based on NOEs because the population of the dimeric state was low and NMR spectra were highly overlapped. The trimeric state was very stable, and, even at a 200:1 DPC:protein ratio, almost 50% of the peptide was present as trimers, precluding direct measurement of the dimer structure.

The conformation of the VEGFR-2tm769 dimer peptide was next studied by covariance analysis of N-H chemical shift changes upon dimerization of WT and mutant TMDs. We plotted the cosine of angle between vectors describing the shift of the signal from the backbone N-H group in the $^{1}H,^{15}N$ transverse relaxation optimized spectroscopy-heteronuclear single quantum coherence (TROSY-HSQC) spectrum (Figure S6), resulting from the dimerization of WT or mutant peptides, versus the ratios of their modules. To balance the contributions from changes in proton and nitrogen shifts, chemical shift changes were measured in hertz. Surprisingly, the vast majority of residues in the hydrophobic helix showed a good correlation for the alteration of amide proton and nitrogen chemical shifts during dimerization, and the signals moved in similar directions and by similar distances in NMR spectra upon dimerization of the WT and the V769E mutant, showing that dimer structures are very similar.

The effect of the amino acid substitution on the structure of VEGFR-2tm769 was further studied in TMD trimers. A concentrated sample (~90% trimer) at a detergent-to-protein ratio of 60 was prepared, and an X-filtered NOESY spectrum was recorded. The quality of this spectrum was poor because of line broadening, which allowed the detection of only seven interhelical contacts. A single set of NMR signals corresponded to the trimeric state, and, therefore, this structure was treated as a symmetric structure where seven interhelical contacts were symmetrized to obtain 21 upper distance restraints, which were used for structure calculation. The resulting structural model is shown in Figure 5B. The trimer interface was compact and located close to the N terminus of the hydrophobic helix. The following residues were involved in helix-helix interactions: $T^{761}xxE^{764}I^{765}xxL^{768}E^{769}xxA^{772}V^{773}xxM^{776}F^{777}xW^{779}L^{780}$. Trimer formation may be additionally supported by stacking of aromatic side chains and by hydrogen bonds formed by the side chains of E769. However, the quality of the obtained structure was too low to determine hydrogen bonding partners for

Table 1. Structural Statistics for the Ensemble of the 10 Best NMR Structures of the VEGFR-2tm and VEGFR-2tm770/777 Dimers and the VEGFR-2tm769 Trimer in DPC Micelles at 318 K and pH 4.5

NMR Distance and Dihedral Restraints			
TM domain	WT	769E	770E/777E
Total unambiguous NOE restraints	418	606	496
Intraresidue	98	150	194
Interresidue	302	435	302
Sequential ($\|i–j\| = 1$)	138	150	116
Medium-range ($1 < \|i–j\| \leq 4$)	164a	285	186
Long-range ($\|i–j\| > 4$)	0	0	0
Intermonomeric	18	21	28
Hydrogen bond restraints (upper/lower)	162/162	243/243	162/162
Total torsion angle restraints	136	204	138
Backbone φ	62	93	62
Backbone ψ	62	93	62
Side chain χ^1	12	18	14
Side chain χ^2	0	0	
Structure Calculation Statistics			
CYANA target function (Å^2)	1.2 ± 0.2	0.5 ± 0.1	4.6 ± 0.2
Restraint violations			
Distance (>0.2 Å)	2	3	8
Distance (>0.3 Å)	0	0	0
Dihedral (>5)°	0	0	1
Average pairwise rmsd (Å)			
α-helical region $(761–794)_2/(761–794)_3$			
Backbone atoms	0.24 ± 0.08	1.5 ± 0.5	0.48 ± 0.23
All heavy atoms	0.74 ± 0.12	2.0 ± 0.4	0.87 ± 0.20
Ramachandran analysis			
% of residues in most favored regions	100.0	87.9	97.1
% of residues in additional allowed regions	0	12.1	2.9
% of residues in generally allowed regions	0	0	0
% of residues in disallowed regions	0	0	0
Helix-Helix Packing			
Contact surface area per monomer in pair of interacting helices (Å^2)	613 ± 20	340 ± 10	847 ± 20
Angle θ between the helix axes (degrees)	25 ± 1	−50 ± 5	55 ± 5, −25 ± 5[a] (18 ± 5)
Distance between the C termini (Å)	15.6 ± 0.6	30.7 ± 4.3	9.6 ± 0.7

[a]The angle between helical axes was calculated separately for N-terminal residues (761–769) and C-terminal residues (778–791) of VEGFR-2tm770/777 because of the bending of the TMD α helix. The angle calculated for the whole TMD helices is given in parentheses.

E769. The overall fold allows this residue to contact the carbonyl group of L768 and the amide group of A772. Geometric parameters of the asymmetric dimer in the trimers were similar to the previously described structures of dimeric TMDs of ErbB2 (Bocharov et al., 2008), ErbB1/ErbB2 (Mineev et al., 2010), and ErbB4 (Bocharov et al., 2012). The angle between the axis of the helices was −50 ± 5°, and the carboxyl termini were separated by 20 Å in active dimers of these kinases based on 3D structures of the extracellular and kinase domains (Jura et al., 2011; Bocharov et al., 2008). Introduction of E769 into the VEGFR-2 TMD does, therefore, not substantially enhance the propensity for dimerization, but it creates an additional surface for helix-helix interactions. We suppose that the observed trimer conformation of this mutant only exists in the VEGFR-2tm769 peptide studied here and does not exist in larger dimeric protein constructs because of steric interference of the ECDs. However, the helix-helix dimer interface observed in VEGFR-2tm769 peptide trimers may reflect the actual conformation of the TMD in the ECD-truncated V769E VEGFR-2 construct.

We next studied the structure of the VEGFR-2tm770/777 peptide carrying two glutamic acid mutations that result in activation of the full-length receptor (Figure 1B). Similar to the WT, two sets of signals were found in the NMR spectra, indicative of two distinct oligomeric states. The presence of the two highly polar glutamic acid residues did not disturb the transmembrane orientation of the peptide (Figure 2), as shown by the number of NOE contacts between the methyl groups of the protein and the methylene groups of the lipid detergent phase (Figure S7). The observed chemical shifts confirm that residues 761–794 form an α helix (Figure 2) with both transmembrane glutamic acid side chains protonated at pH 4.5 and 7.0 (Figure S5). Detergent titration unambiguously revealed two conformational states: one dimeric and the other monomeric, with a free energy of dimerization of −3.2 ± 0.2 kcal/mol, which is substantially lower than the free energy observed for WT VEGFR-2tm dimerization (Figure 3C). Thus, we conclude that VEGFR-2tm770/777 shows a significantly higher dimerization propensity than the WT. Unlike VEGFR-2tm and VEGFR-2tm769, where the dimeric state was relatively rigid, as documented by the narrow signals in the NMR spectra, the spectra of the VEGFR-2tm770/777 dimer contained a number of very broad resonances from both backbone and methyl side chain nuclei (Figure S4C). In particular, a large section of the backbone in the center of the α helix (amino acids 768–779) was characterized by very broad signals in ^{1}H,^{15}N-TROSY-HSQC, whereas several signals from methyl groups in the N-terminal half of the TMD were weak (Figure S4C), suggesting that the backbone of the VEGFR-2tm770/777 dimers perform motions at the microsecond to millisecond time scale, such as twisting, stretching, and bending, that are accompanied by variations in the helix-helix interface.

Analysis of the ^{13}C-filtered-NOESY NMR spectra of VEGFR-2tm770/777 showed 14 intermolecular contacts, which we used to calculate the structure of TMD dimers. Not all intermolecular distance restraints could be satisfied simultaneously in a single NMR structure, as reflected by the relatively high CYANA target function and the bending of the TMD α helix. Therefore, the obtained structure is an average between various conformations of a symmetric (in the NMR time scale) parallel dimer of two α helices (Figure 5C). TMD helices are bent between

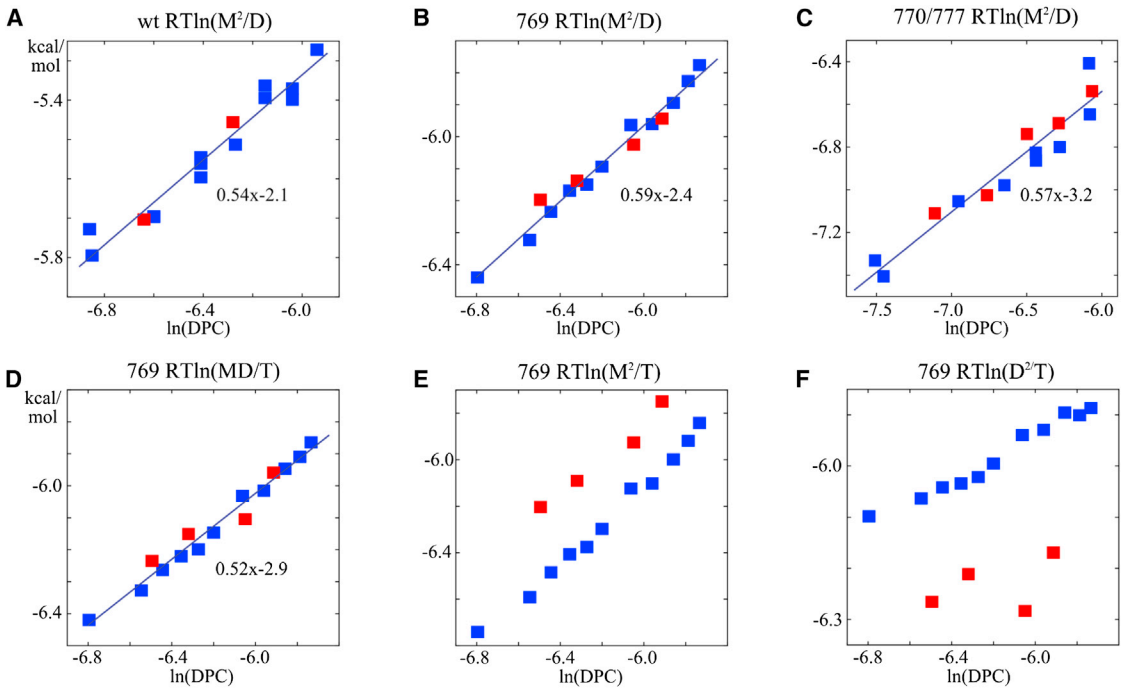

Figure 4. Oligomerization Constants of VEGFR-2 TMD Peptides

(A–F) Apparent free energies of oligomerization were calculated from intensities of signals in $^{1}H,^{15}N$-TROSY-HSQC according to different models of TMD oligomerization for VEGFR-2tm (A), VEGFR-2tm769 (B, dimerization; D, trimerization; E, two dimers; F, tetramerization), and VEGFR-2tm770/777 (C, dimerization) were plotted versus the logarithm of concentration of empty micelles. Red rectangles show data for samples after 2-fold dilution with water. For "true" models, all points show linear dependence of the form $y = ax+b$, where a is γRT (see Supplemental Experimental Procedures) and b is the standard free energy (ΔG_0). The equations describing these dependences are shown in the plots. Standard conditions are 1M of empty DPC micelles at 318 K.

residues 769–778, in agreement with line broadening of the backbone resonances (Figure 5D). The angle between the straight amino- and carboxy-terminal sections of the α helices is ~30°, and the angle between the axes of the TMDs is, therefore, not well defined. The dimer interface involves the following residues: K^{760}xxL^{763}xxI^{766}xV^{769}ExxV^{773}xM^{776}ExxL^{780} LxxI^{784}xxT^{788}. Both glutamic acid residues are on the helix-helix interface and form intermolecular hydrogen bonds with the backbone of the opposing helix. However, the quality of the NMR spectra is insufficient to determine the precise partner amino acids. The helix-helix interface of the activating VEGFR-2tm770/777 peptide is on the opposite side of the interface of the WT TMD, in agreement with the observed chemical shifts of the methyl groups. In particular, the δ-methyl side chains of L763 in the mutant differ from those of VEGFR-2tm, which cannot be explained by the changes in the intramolecular environment resulting from the introduction of glutamic acid in positions 770 and 777 (Figures S4A and S4C). Moreover, the free energy of dimerization of VEGFR-2tm770/777 is insensitive to the protonation state of E764, consistent with the fact that this residue is not part of the dimerization interface (Figures 5C and 5D). This clearly distinguishes the activating VEGFR-2tm770/777 from WT VEGFR-2tm and VEGFR-2tm769.

Taken together, three major aspects distinguish the VEGFR-2tm770/777 dimer from the WT. Dimerization propensity is enhanced by ~1 kcal/mol; dimerization occurs via a completely different interface lying on the opposite face of the helix; and the structure of this dimer is flexible, which means that TMD helices can bend and perform motions at a microsecond to millisecond time scale.

MD Simulations of WT and Mutant TMD Dimers

Analysis of the trajectories for the WT TMDs shows that this system is remarkably stable (Figure 6, black trace), maintaining the interhelical aromatic and hydrophobic packing observed in the NMR structure with only minor fluctuations of the side chains. Interestingly, this is not the case in the simulation of the constitutively active G770E/F777E mutant, where the TMDs rapidly undergo significant structural changes from their starting conformation (Figure 6, red trace). Specifically, we observe that residues 770 and 777 mutated to glutamic acid engage in an interhelical "glutamic acid zipper" that stabilizes sliding of the TMDs by ~5 Å (Figure 7; Movie S1). This behavior agrees with the NMR data showing that the structure of this mutant is flexible, with motions promoting changes in the dimerization interface.

We next asked whether these structural rearrangements are also possible in the WT receptor by running an MD simulation of a model of the WT TMD built on the NMR structure of the G770E/F777E mutant. The trajectories show that this system is relatively unstable and undergoes large structural rearrangements, even at relatively short time scales (Figure 6, orange trace). A more detailed analysis shows a rapid rearrangement in the aromatic dimerization interface because of a change in

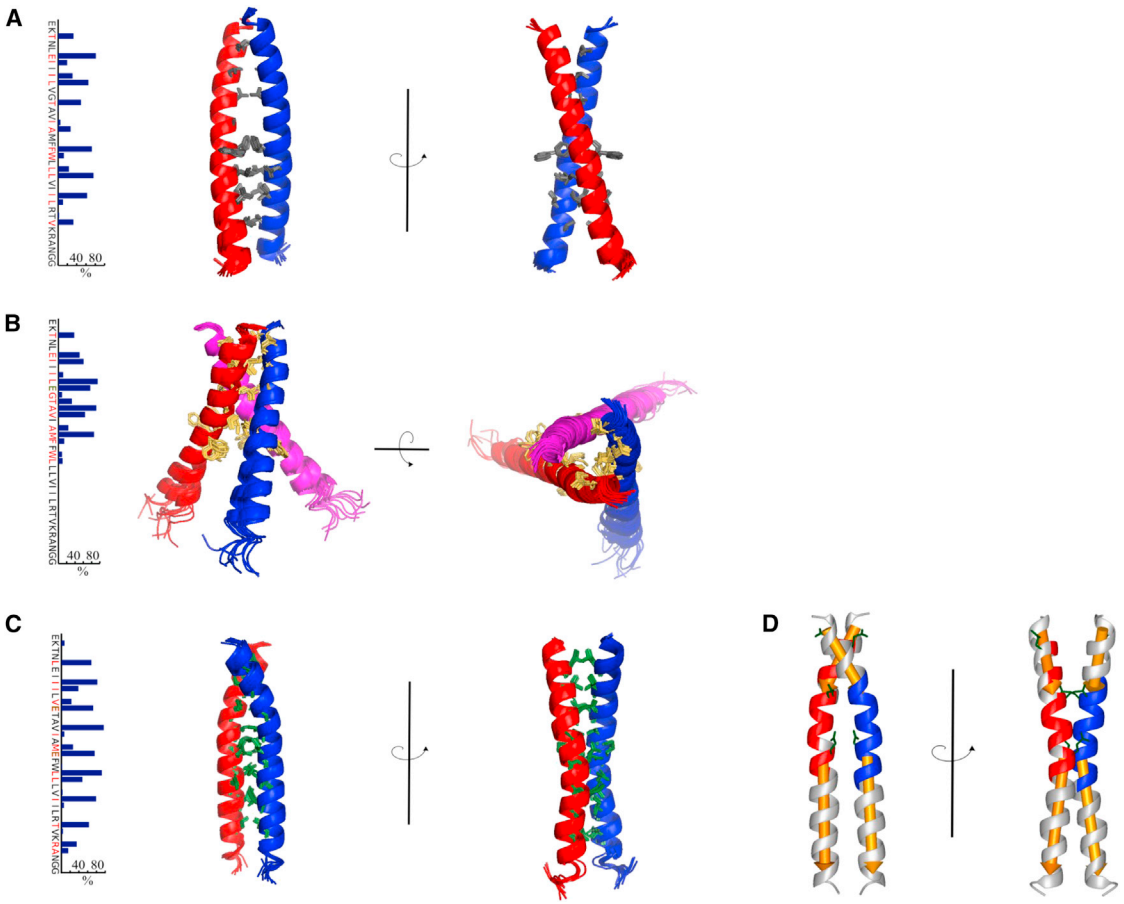

Figure 5. Structure of VEGFR-2 TMD Peptides

(A–C) The ten best NMR structures (shown as ribbons) were superimposed using the backbone atoms. Side chains of residues on the dimerization interface are shown as gray (A), yellow (B), and green (C) sticks. The intermonomeric contact surface area of VEGFR-2 TMDs is shown as the percentage of the total solvent-accessible area in the graphs in the left margin.

(D) Bending of double glutamic acid mutated TMD helix along the axis.

side chain conformation of F777, which is accompanied by a small rotation and sliding of the TMDs that, together, optimize the aromatic interactions. However, this seemingly minor rearrangement brings the basic residues R787, K790, and R791 in close proximity at the cytoplasmic side of the helices. As a result, the C-terminal ends of the TMDs move ~15 Å apart, thereby minimizing the electrostatic repulsion between these positively charged residues (Figure 8; Movie S2). These large rearrangements are likely not biologically relevant for WT VEGFR-2 activation and simply result from the lack of a stabilizing mechanism of the active arrangement in the WT sequence, e.g., the glutamic acid zipper in the G770E/F777E mutant (Figure 7) or from VEGF-mediated interactions in the ECDs of the full-length WT receptor.

In the absence of NMR data for the inactivating I774E/L781E mutant, we tested the possible impact of these mutations using the WT conformation as a template for MD simulation. We found that E774 and E781 do not engage in interhelical interactions and that the hydrophobic and aromatic dimerization interfaces were maintained during simulation. Therefore, this system remains remarkably stable (Figure 6, blue trace). We consider the high stability of this conformation, which is similar to the WT, to be the reason for the inactive phenotype of this mutant.

DISCUSSION

Transmembrane signaling by RTKs requires specific orientation of the intracellular kinase domains in active receptor dimers. Earlier studies showed that replacing small hydrophobic residues with polar amino acids in the TMD, as observed, for instance, in naturally occurring FGFR mutants, causes severe developmental pathologies, such as Crouzon syndrome, achondroplasia, or oncogenic transformation (Li et al., 2006; Webster and Donoghue, 1996; Li et al., 1997). This results from a decrease in the free energy of dimerization by approximately 1.3 kcal/mol (Chen et al., 2010b). Similar mutations observed in Neu receptors led to oncogenic transformation (Bargmann and Weinberg, 1988). Based on these observations, constitutively active PDGFR-β, Neu (Bell et al., 2000), and VEGFR-2 (Dosch and Ballmer-Hofer, 2010) mutants were generated that carry dimerization-promoting TMDs consisting of 23 valine and 2 glutamic acid residues. All mutants gave rise to constitutive

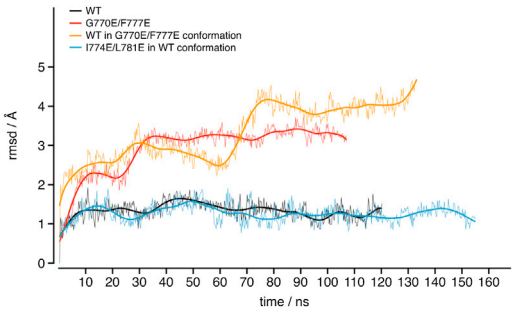

Figure 6. Root-Mean-Square Deviation of the Cα Atoms from the Initial Structure in the MD Simulations

The NMR structure of the WT TMDs (black trace) and the model of the I774E/L781E mutant built on this structure (blue trace) stabilize rapidly in a conformation very close to the starting structure. Thus, these arrangements of the TMDs likely represent stable local minima. However, the NMR structure of the G770E/F777E mutant (red trace) and the model of the WT sequence built on this structure (orange trace) rapidly undergo significant conformational changes that lead these systems to adopt different relative arrangements of the TMDs.

receptor dimers, yet only a small subset showed increased ligand-independent activity, illustrating that dimerization is necessary, but not sufficient, for activation. Here we further applied scanning mutagenesis to the TMD of VEGFR-2 and determined the activity of mutant constructs and the exact spatial conformation of transmembrane helix dimers.

Kinase activity was increased in ECD-deleted VEGFR-2 compared with the full-length receptor, and this activity was increased further upon mutation of either I767, L768, or V796 to glutamic acid. However, a single polar amino acid mutation did not activate the full-length receptor, presumably because the change in the free energy of dimerization was too small to compensate for receptor repulsion by the ECD and/or negative steric interference between the TMD and the ligand-bound ECD. Taken together, this suggests that, in the absence of ligand, the ECD impedes receptor activation, maintaining receptors in an inactive conformation, as shown earlier for EGFR (Ferguson et al., 2003) and FGFR (Chen et al., 2010b).

Therefore, we generated double glutamic acid TMD VEGFR-2 mutants. G770E/F777E and I771E/L778E displayed constitutively high ligand-independent activity. In agreement with earlier publications, this demonstrates that TMDs carrying two polar amino acids show a high dimerization propensity and, when the mutant residues are correctly positioned, activate RTKs (Bell et al., 2000; Dosch and Ballmer-Hofer, 2010). A thermodynamic analysis of ligand binding to the ECD of VEGFR-2 showed that homotypic interactions in the membrane-proximal part of the receptor ECD destabilize ligand-receptor dimers by

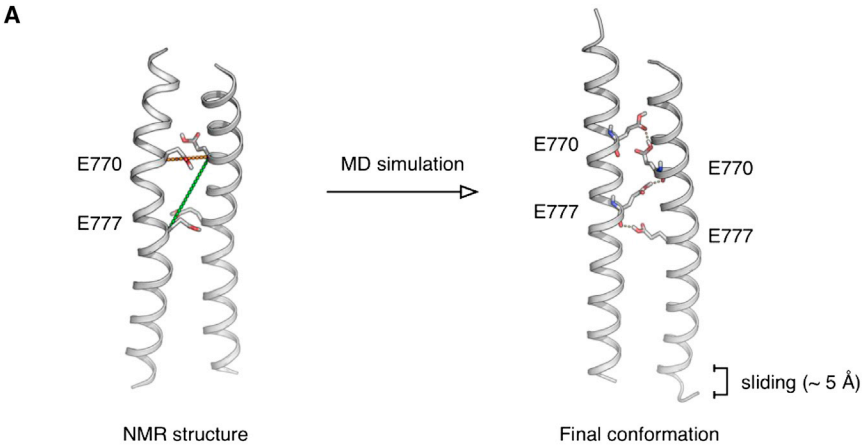

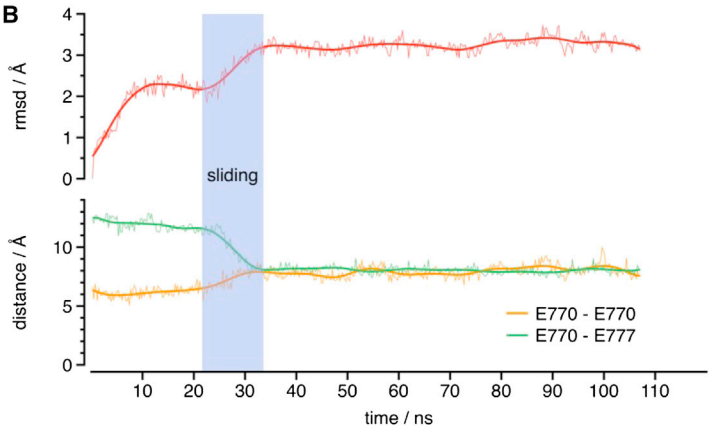

Figure 7. Structural Rearrangements in the G770E/F777E Mutant Observed in MD Simulations

(A) NMR structure of the G770E/F777E mutant TMD peptide (left) and final structure in the MD simulation (right). Structural rearrangements during the simulation result in the formation of a glutamic acid zipper (hydrogen bonds are shown as broken lines) and sliding of the TMDs relative to each other.

(B) Sliding can be observed as a significant conformational change early in the simulation (e.g., in the root-mean-square deviation [rmsd] profile, red trace) that can be quantified by measuring the distances between E770 and E777 in opposite helices [green and orange lines in (A), left, and traces in (B)]. See also Movie S1.

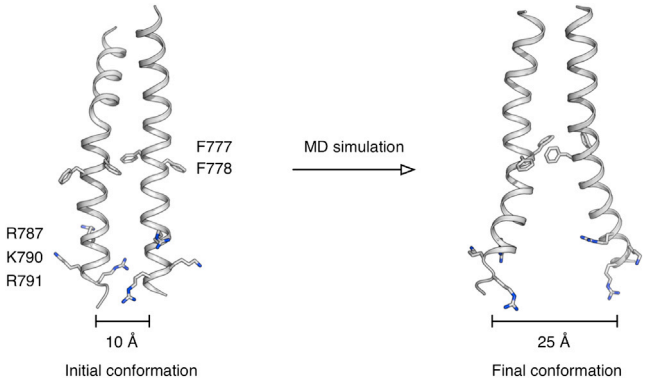

Figure 8. Structural Rearrangements in the WT TMD Observed in MD Simulations

The model on the left shows the active conformation of WT TMDs. This structure has the same dimerization interface as the NMR structure of the G770E/F777E double mutant (Figure 5C), with the exception of the contacts mediated by residues 770 and 777. On the right, MD simulations show that relocation of the interhelical aromatic-aromatic interactions mediated by F777 and F778 in the WT TMD peptide results in a small helix sliding and rotation that is further amplified into a large rearrangement of the helix C-terminal domains. These regions move 15 Å apart in the course of the simulation, to a final distance of 25 Å. See also Movie S2. Thus, the absence of the glutamic acid zipper in the WT TMDs (compare with Figure 7) increases structural flexibility.

1.0−1.7 kcal/mol (Brozzo et al., 2012). Because the V769E mutant only insignificantly decreased the free energy of dimerization, our data explain why a second polar residue is required for constitutive dimer formation of VEGFR-2. This is in full agreement with similar thermodynamic data published for FGFR3, showing that two glutamic acid residues are required to stabilize receptor dimers by the TMD (Chen et al., 2010a; Chen et al., 2010b). Taken together, this shows that, in the absence of ligand, the ECD acts as an energy barrier that prevents ligand-independent VEGFR-2 activation. We propose that this proofreading mechanism is biologically relevant to ensure tight control of VEGF signaling.

Investigating the structural changes caused by glutamic acid mutation of RTK TMDs, Bell et al. (2000) proposed a model in which the rotational angle at which kinase subunits interact with each other governs receptor activation. To identify the TMD dimer structure required for kinase activation, we determined the structures of WT (VEGFR-2tm), single mutant (VEGFR-2tm769), and double mutant (VEGFR-2tm770/777) TMD peptides in DPC micelles applying NMR spectroscopy. We found three distinct TMD conformations. The first conformation represents the dimeric structure of the inactive WT VEGFR-2tm. VEGFR-2tm770/777, representing the activating TMD, differed from the WT dimer conformation because of rotation of the helices by 180°. This suggests that the WT dimer structure is either functionally meaningless or corresponds to an inactive, predimerized state of VEGFR-2 as, for instance, observed for EGFRs (Tao and Maruyama, 2008). This is supported by the high stability of the WT dimer (−4.6 kcal/mol at 1M of detergent) compared with TMDs of other RTKs (Finger et al., 2009). In addition, MD simulation of the I774E/L781E TMD in the context of the WT dimer structure maintained the native hydrophobic and aromatic dimerization interface observed in the NMR structure (Figure 6). In agreement with the simulation of the active G770E/F777E mutant, E774 and E781 did not form interhelical interactions, possibly because the stable and bulky aromatic cluster formed by F777, F778, and W779 localized in between the two mutant residues. The aromatic residues sterically prevent helices from rotating and sliding into an alternative conformation and, thus, trap the helices in the inactive WT conformation. As a consequence, I774E/L781E substitutions render VEGFR-2 constitutively inactive because of stabilization of the WT dimerization interface. Therefore, we favor the idea that this WT dimeric structure represents the conformation of the receptor in a predimerized, inactive state.

A second conformation was found for the VEGFR-2tm770/777 mutant and represents the active state of the full-length VEGFR-2, as confirmed by our biochemical analysis. The positions of the glutamic acid residues in the activating (G770E/F777E) and the inactivating (I774E/L781E) double mutants agree well with our data published earlier using all valine TMDs of VEGFR-2 (Dosch and Ballmer-Hofer, 2010). These conformations are stable enough to promote constitutive dimerization of VEGFR-2, and G770E/F777E provides the free energy required to compensate for steric repulsion by the receptor ECD. We further studied the molecular details of the dimerization interface of TMDs by MD simulation and modeled the conformations for interhelical interactions. Such changes occur on a nanosecond time scale (Henzler-Wildman and Kern, 2007), so they can be captured in our simulations, which range between 120−150 ns. We found a number of interaction patterns and identified specific residues that are key to understanding the molecular determinants responsible for the phenotype of the G770E/F777E mutant. Glutamic acid residues 770 and 777 engage in a glutamic acid zipper that stabilizes the relative sliding of the TMDs by ~5 Å. Such a sliding may be part of the motions suggested by the NMR data, and it would also provide an additional source of asymmetry probably required for receptor activation. We also propose that phenylalanine 777 is a key regulator of the dimerization interface because changes in side chain conformation of this residue are often related to larger-scale rearrangements of the TMD. The MD simulations thus suggest that, in addition to the rotation of the TMDs relative to each other observed in the NMR structure of the constitutively active VEGFR mutant, additional dynamic properties, such as sliding of the helices, may be important for receptor activation.

A third conformation was observed in the V769E mutant TMD and was derived from the peptide trimer structure. There is, however, no evidence that such trimers are biologically relevant and exist in the context of VEGFR-2 kinase constructs. V769E substitution has clear biological consequences for activation of the ECD-deleted VEGFR-2 construct, which is reflected neither in an enhancement of the TMD dimerization propensity nor in establishing a preferred dimeric conformation. Therefore, we propose that the observed symmetric trimer structure describes the pairwise helix-helix interactions present in constitutively active, ECD-truncated V769E VEGFR-2 dimers. The symmetric trimer structure may, however, give some insight into pairwise helix-helix interactions. This conformation may allow for optimal arrangement of the intracellular kinase domains but is

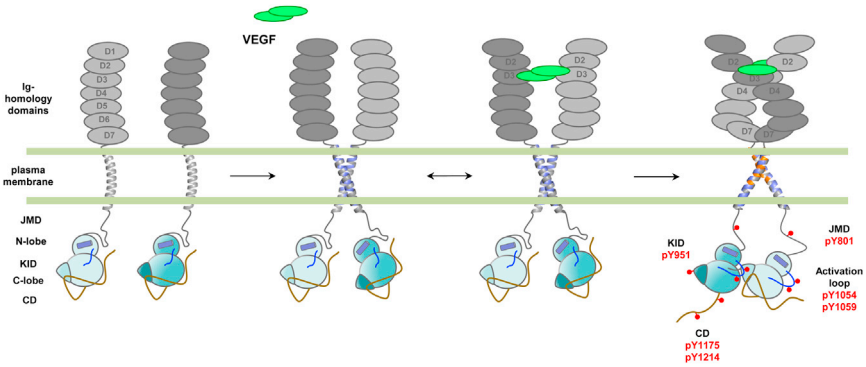

Figure 9. Model of VEGF Receptor Activation
for details, see main text).

incompatible with full-length constructs and does not promote the long-lived asymmetric state of activating TMDs (Figure 5B; Figure S8).

Because our structural analysis was performed with isolated micelle-embedded peptidic TMDs, our conclusions may not be unanimously applicable to the structure of full-length receptor constructs. However, because the effect of the mutations on the activity of VEGFR-2 agrees well with the observed structures of TMD dimers, we are confident that our structural analysis is also applicable to full-length receptors. In the absence of data for full-length receptor constructs, our conclusions are consistent and may provide relevant insights into the role of the TMD in VEGFR-2 activation.

Taken together, we describe here a mechanism for VEGFR-2 activation that relies on two alternative TMD conformations, WT and G770E/F777E. Comparing the structures of these TMDs shows the reorientation of the mutant by rotating both helices along the helical axis by 180°. We propose the mechanism of receptor activation summarized in Figure 9 and Figure S8. In the absence of ligand, the ECD maintains the receptor in an inactive state, and receptor monomers exist in a dynamic monomer-dimer equilibrium that is regulated by the intrinsic dimerization propensity of the WT TMD. This preformed dimer may lower the activation energy of the receptor. Ligand binding and subsequent formation of homotypic receptor ECD contacts leads to the rotation of TMD helices by 180° relative to the inactive WT conformation, presumably accompanied by sliding of the TMDs relative to each other. Auto- and transphosphorylation of tyrosine residues in the kinase and the carboxy-terminal receptor domain activates downstream signaling.

VEGF signaling is tightly controlled in vasculogenesis and angiogenesis, as demonstrated by the embryonic lethality observed upon VEGFR-2 ablation and heterozygous inactivation of VEGF-A (Shalaby et al., 1997; Shalaby et al., 1995; Ferrara et al., 1996). So far, disease-related, constitutively active VEGFR-2 was only found in juvenile hemangiomas, resulting from missense mutations in VEGFR-2, that lead to the downregulation of the inhibitory soluble variant of VEGFR-1 (Jinnin et al., 2008). Tight control of VEGFR-2 activity is therefore critical for vessel homeostasis and might be the consequence of the inhibitory activity exerted by the receptor ECD (Brozzo et al., 2012), which prevents aberrant dimerization in the absence of ligand. We believe that future structural and functional information on active, inactive, and transition-state dimeric TMD conformations will open novel possibilities for the design of compounds targeting the hydrophobic milieu of the TMD.

EXPERIMENTAL PROCEDURES

Construction of Human VEGFR-2 TMD Mutants

TMD mutants were cloned by introducing single or double glutamic acid mutations into the WT TMD. As described before, all constructs were tagged with an amino-terminal hemagglutinin (HA) sequence as described (Dosch and Ballmer-Hofer, 2010). A summary of all mutants is given in Figure S1.

Cell Culture and Kinase Activity Determination

HEK293 cell cultures were maintained and kinase activities were determined as described (Dosch and Ballmer-Hofer, 2010) using the phospho-specific antibody pY1175 (Cell Signaling Technology) and an antibody recognizing the HA-tagged constructs (clone 3F10, Roche Diagnostics).

Cell-free Expression and Purification of VEGFR-2 TMD Peptides for NMR Analysis

The nucleic acid sequences encoding the TMD peptides for the WT VEGFR-2-tm peptide (MEKTNLEIIILVGTAVIAMFFWLLLVIILRTVKRANGG), the single mutant VEGFR-2-tm769 (MEKTNLEIIILE^{769}G TAVIAMFFWLLLVIILRTVKRANGG), and the double mutant VEGFR-2-tm770/777 (MEKTNLEIIILVE^{770}TAVIAME^{777}FWLLLVIILR TVKRANGG) (all numbering according to P35968, UniProt database, and the predicted TMD helix is underlined) were cloned into the pET20b(+) vector (Novagen) at NdeI and HindIII. The resulting plasmids were named pET20b(+)/TMD-VEGFR-2 and pET20b(+)/TMD-VEGFR-2(V^{769} to glutamic acid), respectively. All proteins were synthesized in the continuous exchange cell-free expression system based on *E. coli* S30 extracts (Mineev et al., 2011; Bocharov et al., 2010).

NMR Spectroscopy and Calculation of Spatial Structures

NMR spectra were acquired at 45°C on a 600-MHz Avance III spectrometer (Bruker BioSpin) equipped with pulsed-field gradient, triple resonance cryoprobes. The backbone and side chain ^{1}H, ^{13}C, and ^{15}N resonances were assigned using standard triple resonance techniques (Cavanagh, 2007) in the CARA software (Keller, 2004). Triple resonance spectra were acquired in a sparse sampling mode and processed with qMDD software (Orekhov and Jaravine, 2011). NMR spatial structures of the VEGFR-2tm and VEGFR-2tm770/777 homodimer and VEGFR-2tm769 homotrimer were calculated using the CYANA program (Guentert, 2003). Assignment of the experimental restraints and structure calculation was performed as described previously (Bocharov et al., 2008; Bocharov et al., 2007).

Analysis of NMR Chemical Shifts

To investigate the spatial structure of the VEGFR-2tm769 dimer, we determined NMR chemical shifts. For this purpose, the shifts of NMR signals in ^{1}H,^{15}N-TROSY-HSQC occurring upon TMD dimerization were considered. Shifts were characterized by vectors with coordinates $\Delta\delta\cdot\Omega_H\Delta\delta\cdot\Omega_H$ and $\Delta\delta\cdot\Omega_N\Delta\delta\cdot\Omega_N$, where $\Delta\delta\Delta\delta$ and $\Delta\delta\Delta\delta$ are changes in ^{1}H and ^{15}N chemical shifts, whereas $\Omega_H\Omega_H$ and $\Omega_N\Omega_N$ are their Larmor frequencies. For two peptides (VEGFR-2tm and VEGFR-2tm769), such vectors were calculated for each residue, with the unambiguously determined assignment of dimeric and monomeric states, and the cosine of angle between these two vectors was plotted versus the ratio of their modules to study the correlations in the N-H chemical shift changes. Intermonomeric NOE contacts were identified directly from the 3D ^{15}N,^{13}C F1-filtered/F3-edited NOESY spectra (for details, see Supplemental Experimental Procedures).

Determination of the Oligomeric State and Oligomerization Free Energy of VEGFR-2 TMDs

To determine the oligomeric states of VEGFR-2tm, VEGFR-2tm 770/777, and VEGFR-2tm769 and to measure the corresponding free energies of dimerization and oligomerization, initial samples were diluted either with concentrated DPC solution or distilled water to vary both the DPC concentration and the protein/DPC ratio. At each point, a $^{1}H,^{15}N$-TROSY-HSQC spectrum was recorded. Populations of oligomeric states, aggregation numbers for the oligomeric states of VEGFR-2tm769, and the corresponding free energies of dimerization/oligomerization equilibria were determined as described by Mineev et al. (2014).

Molecular Dynamics Simulations

The NMR structures of the WT and G770E/F777E mutant TMDs (residues 759–795) were used as initial coordinates for MD simulations. First, the protonation state of titratable groups (except for glutamic acids, which were set as neutral as measured by NMR) were calculated using PROPKA (Olsson et al., 2000) at pH 7.0, as implemented in Protein Data Bank ID code 2PQR (Dolinsky et al., 2004). The TMDs were then inserted in a hydrated lipid bilayer composed of approximately 130 palmitoyl-oleoyl-phosphatidyl-choline molecules and 3,700 water molecules. Ions were added to a concentration of 0.15 M NaCl, and additional ions were added to achieve charge neutrality. The system measured roughly 50 × 50 × 80 $Å^3$, with a total of approximately 23,000 atoms. This system was equilibrated as follows. First, a short (0.5-ns) simulation was performed, in which only the lipid tails were allowed to move to induce the appropriate disorder of a fluid-like bilayer. Next, the geometry of the entire system was optimized by energy minimization, followed by equilibration steps with the protein constrained (0.5 ns) and without constraints (0.5 ns). Simulations were carried out using NAMD 2.8 (Phillips et al., 2005) with the CHARMM27 all-hydrogen force field (MacKerell et al., 1998) at constant temperature (300 K) and pressure (1 atmosphere) and using a time step of 2 femtosecond.

SUPPLEMENTAL INFORMATION

Supplemental Information includes Supplemental Experimental Procedures, eight figures, and two movies and can be found with this article online at http://dx.doi.org/10.1016/j.str.2014.05.010.

AUTHOR CONTRIBUTIONS

K.B.H. initiated and supervised the project and wrote the article. S.M. made the receptor constructs, analyzed receptor activity, and wrote the article. M.M. performed the MD simulations. X.D. performed MD simulations and wrote the paper. K.S.M. performed NMR experiments and the calculation of spatial structures and wrote the article. A.S.A. supervised the project and wrote the article. E.N.L. and M.A.S. designed expression vectors, developed the protocols, and performed cell-free expression. M.P.K. analyzed and managed cell-free expression.

ACKNOWLEDGMENTS

We thank the Swiss National Science Foundation (grants 31003A-130463 to K.B.H. and 31003A-146520 to X.D.), Oncosuisse (grant OC2 01200-08-2007 to K.B.H.), the NOVARTIS Stiftung für Medizinisch-Biologische Forschung (grant 10C61 to K.B. H.), the Russian Foundation for Basic Research (grants 12-04-01816 to A.S.A. and 12-04-31027 to K.S.M.), and the Russian Academy of Sciences (Program "Molecular and Cellular Biology: to A.S.A.) for support. Molecular dynamics simulations were run at the Swiss National Supercomputing Centre (CSCS). We thank Kate Thieltges for technical assistance.

Received: October 29, 2013
Revised: May 16, 2014
Accepted: May 17, 2014
Published: June 26, 2014

REFERENCES

Bae, J.H., Boggon, T.J., Tomé, F., Mandiyan, V., Lax, I., and Schlessinger, J. (2010). Asymmetric receptor contact is required for tyrosine autophosphorylation of fibroblast growth factor receptor in living cells. Proc. Natl. Acad. Sci. USA *107*, 2866–2871.

Bargmann, C.I., and Weinberg, R.A. (1988). Oncogenic activation of the neu-encoded receptor protein by point mutation and deletion. EMBO J. *7*, 2043–2052.

Barton, W.A., Tzvetkova-Robev, D., Miranda, E.P., Kolev, M.V., Rajashankar, K.R., Himanen, J.P., and Nikolov, D.B. (2006). Crystal structures of the Tie2 receptor ectodomain and the angiopoietin-2-Tie2 complex. Nat. Struct. Mol. Biol. *13*, 524–532.

Bell, C.A., Tynan, J.A., Hart, K.C., Meyer, A.N., Robertson, S.C., and Donoghue, D.J. (2000). Rotational coupling of the transmembrane and kinase domains of the Neu receptor tyrosine kinase. Mol. Biol. Cell *11*, 3589–3599.

Bocharov, E.V., Pustovalova, Y.E., Pavlov, K.V., Volynsky, P.E., Goncharuk, M.V., Ermolyuk, Y.S., Karpunin, D.V., Schulga, A.A., Kirpichnikov, M.P., Efremov, R.G., et al. (2007). Unique dimeric structure of BNip3 transmembrane domain suggests membrane permeabilization as a cell death trigger. J. Biol. Chem. *282*, 16256–16266.

Bocharov, E.V., Mineev, K.S., Volynsky, P.E., Ermolyuk, Y.S., Tkach, E.N., Sobol, A.G., Chupin, V.V., Kirpichnikov, M.P., Efremov, R.G., and Arseniev, A.S. (2008). Spatial structure of the dimeric transmembrane domain of the growth factor receptor ErbB2 presumably corresponding to the receptor active state. J. Biol. Chem. *283*, 6950–6956.

Bocharov, E.V., Mayzel, M.L., Volynsky, P.E., Mineev, K.S., Tkach, E.N., Ermolyuk, Y.S., Schulga, A.A., Efremov, R.G., and Arseniev, A.S. (2010). Left-handed dimer of EphA2 transmembrane domain: Helix packing diversity among receptor tyrosine kinases. Biophys. J. *98*, 881–889.

Bocharov, E.V., Mineev, K.S., Goncharuk, M.V., and Arseniev, A.S. (2012). Structural and thermodynamic insight into the process of "weak" dimerization of the ErbB4 transmembrane domain by solution NMR. Biochim. Biophys. Acta *1818*, 2158–2170.

Bocharov, E.V., Lesovoy, D.M., Goncharuk, S.A., Goncharuk, M.V., Hristova, K., and Arseniev, A.S. (2013). Structure of FGFR3 transmembrane domain dimer: implications for signaling and human pathologies. Structure *21*, 2087–2093.

Brozzo, M.S., Bjelić, S., Kisko, K., Schleier, T., Leppänen, V.M., Alitalo, K., Winkler, F.K., and Ballmer-Hofer, K. (2012). Thermodynamic and structural description of allosterically regulated VEGFR-2 dimerization. Blood *119*, 1781–1788.

Cavanagh, J. (2007). Protein NMR spectroscopy: Principles and practice. (Amsterdam: Academic Press).

Chen, L., Novicky, L., Merzlyakov, M., Hristov, T., and Hristova, K. (2010a). Measuring the energetics of membrane protein dimerization in mammalian membranes. J. Am. Chem. Soc. *132*, 3628–3635.

Chen, L., Placone, J., Novicky, L., and Hristova, K. (2010b). The extracellular domain of fibroblast growth factor receptor 3 inhibits ligand-independent dimerization. Sci. Signal. *3*, ra86.

Dolinsky, T.J., Nielsen, J.E., McCammon, J.A., and Baker, N.A. (2004). PDB2PQR: an automated pipeline for the setup of Poisson-Boltzmann electrostatics calculations. Nucleic Acids Res. *32*, W665–W667.

Dosch, D.D., and Ballmer-Hofer, K. (2010). Transmembrane domain-mediated orientation of receptor monomers in active VEGFR-2 dimers. FASEB J. *24*, 32–38.

Endres, N.F., Das, R., Smith, A.W., Arkhipov, A., Kovacs, E., Huang, Y., Pelton, J.G., Shan, Y., Shaw, D.E., Wemmer, D.E., et al. (2013). Conformational coupling across the plasma membrane in activation of the EGF receptor. Cell *152*, 543–556.

Ferguson, K.M., Berger, M.B., Mendrola, J.M., Cho, H.S., Leahy, D.J., and Lemmon, M.A. (2003). EGF activates its receptor by removing interactions that autoinhibit ectodomain dimerization. Mol. Cell *11*, 507–517.

Ferrara, N., Carver-Moore, K., Chen, H., Dowd, M., Lu, L., O'Shea, K.S., Powell-Braxton, L., Hillan, K.J., and Moore, M.W. (1996). Heterozygous embryonic lethality induced by targeted inactivation of the VEGF gene. Nature *380*, 439–442.

Finger, C., Escher, C., and Schneider, D. (2009). The single transmembrane domains of human receptor tyrosine kinases encode self-interactions. Sci. Signal. *2*, ra56.

Guentert, P. (2003). Automated NMR protein structure calculation. Prog. Nucl. Magn. Reson. Spectrosc. *43*, 105–125.

Gullick, W.J., Bottomley, A.C., Lofts, F.J., Doak, D.G., Mulvey, D., Newman, R., Crumpton, M.J., Sternberg, M.J., and Campbell, I.D. (1992). Three dimensional structure of the transmembrane region of the proto-oncogenic and oncogenic forms of the neu protein. EMBO J. *11*, 43–48.

Henzler-Wildman, K., and Kern, D. (2007). Dynamic personalities of proteins. Nature *450*, 964–972.

Hyde, C.A., Giese, A., Stuttfeld, E., Abram, S.J., Villemagne, D., Schleier, T., Binz, H.K., and Ballmer-Hofer, K. (2012). Targeting the extracellular domains D4 and D7 of VEGFR-2 reveals allosteric receptor regulatory sites. Mol. Cell. Biol. *32*, 3802–3813.

Jinnin, M., Medici, D., Park, L., Limaye, N., Liu, Y., Boscolo, E., Bischoff, J., Vikkula, M., Boye, E., and Olsen, B.R. (2008). Suppressed NFAT-dependent VEGFR1 expression and constitutive VEGFR2 signaling in infantile hemangioma. Nat. Med. *14*, 1236–1246.

Jura, N., Endres, N.F., Engel, K., Deindl, S., Das, R., Lamers, M.H., Wemmer, D.E., Zhang, X., and Kuriyan, J. (2009). Mechanism for activation of the EGF receptor catalytic domain by the juxtamembrane segment. Cell *137*, 1293–1307.

Jura, N., Zhang, X., Endres, N.F., Seeliger, M.A., Schindler, T., and Kuriyan, J. (2011). Catalytic control in the EGF receptor and its connection to general kinase regulatory mechanisms. Mol. Cell *42*, 9–22.

Kelleher, F.C., O'Sullivan, H., Smyth, E., McDermott, R., and Viterbo, A. (2013). Fibroblast growth factor receptors, developmental corruption and malignant disease. Carcinogenesis *34*, 2198–2205.

Keller, R.L.J. (2004). The Computer Aided Resonance Assignment Tutorial. (Goldau: Cantina Verlag).

Kisko, K., Brozzo, M.S., Missimer, J., Schleier, T., Menzel, A., Leppänen, V.M., Alitalo, K., Walzthoeni, T., Aebersold, R., and Ballmer-Hofer, K. (2011). Structural analysis of vascular endothelial growth factor receptor-2/ligand complexes by small-angle X-ray solution scattering. FASEB J. *25*, 2980–2986.

Koch, S., Tugues, S., Li, X., Gualandi, L., and Claesson-Welsh, L. (2011). Signal transduction by vascular endothelial growth factor receptors. Biochem. J. *437*, 169–183.

Lemmon, M.A., and Ferguson, K.M. (2007). A new twist in the transmembrane signaling tool-kit. Cell *130*, 213–215.

Leppänen, V.M., Prota, A.E., Jeltsch, M., Anisimov, A., Kalkkinen, N., Strandin, T., Lankinen, H., Goldman, A., Ballmer-Hofer, K., and Alitalo, K. (2010). Structural determinants of growth factor binding and specificity by VEGF receptor 2. Proc. Natl. Acad. Sci. USA *107*, 2425–2430.

Leppänen, V.M., Tvorogov, D., Kisko, K., Prota, A.E., Jeltsch, M., Anisimov, A., Markovic-Mueller, S., Stuttfeld, E., Goldie, K.N., Ballmer-Hofer, K., and Alitalo, K. (2013). Structural and mechanistic insights into VEGF receptor 3 ligand binding and activation. Proc. Natl. Acad. Sci. USA *110*, 12960–12965.

Li, Y., Mangasarian, K., Mansukhani, A., and Basilico, C. (1997). Activation of FGF receptors by mutations in the transmembrane domain. Oncogene *14*, 1397–1406.

Li, E., You, M., and Hristova, K. (2006). FGFR3 dimer stabilization due to a single amino acid pathogenic mutation. J. Mol. Biol. *356*, 600–612.

Liu, H., Chen, X., Focia, P.J., and He, X. (2007). Structural basis for stem cell factor-KIT signaling and activation of class III receptor tyrosine kinases. EMBO J. *26*, 891–901.

MacKerell, A.D., Bashford, D., Bellott, M., Dunbrack, R.L., Evanseck, J.D., Field, M.J., Fischer, S., Gao, J., Guo, H., Ha, S., et al. (1998). All-atom empirical potential for molecular modeling and dynamics studies of proteins. J. Phys. Chem. B *102*, 3586–3616.

Mi, L.Z., Lu, C., Li, Z., Nishida, N., Walz, T., and Springer, T.A. (2011). Simultaneous visualization of the extracellular and cytoplasmic domains of the epidermal growth factor receptor. Nat. Struct. Mol. Biol. *18*, 984–989.

Mineev, K.S., Bocharov, E.V., Pustovalova, Y.E., Bocharova, O.V., Chupin, V.V., and Arseniev, A.S. (2010). Spatial structure of the transmembrane domain heterodimer of ErbB1 and ErbB2 receptor tyrosine kinases. J. Mol. Biol. *400*, 231–243.

Mineev, K.S., Khabibullina, N.F., Lyukmanova, E.N., Dolgikh, D.A., Kirpichnikov, M.P., and Arseniev, A.S. (2011). Spatial structure and dimer—monomer equilibrium of the ErbB3 transmembrane domain in DPC micelles. Biochim. Biophys. Acta *1808*, 2081–2088.

Mineev, K.S., Lesovoy, D.M., Usmanova, D.R., Goncharuk, S.A., Shulepko, M.A., Lyukmanova, E.N., Kirpichnikov, M.P., Bocharov, E.V., and Arseniev, A.S. (2014). NMR-based approach to measure the free energy of transmembrane helix-helix interactions. Biochim. Biophys. Acta *1838* (1 Pt B), 164–172.

Ogiso, H., Ishitani, R., Nureki, O., Fukai, S., Yamanaka, M., Kim, J.H., Saito, K., Sakamoto, A., Inoue, M., Shirouzu, M., and Yokoyama, S. (2002). Crystal structure of the complex of human epidermal growth factor and receptor extracellular domains. Cell *110*, 775–787.

Opatowsky, Y., Lax, I., Tomé, F., Bleichert, F., Unger, V.M., and Schlessinger, J. (2014). Structure, domain organization, and different conformational states of stem cell factor-induced intact KIT dimers. Proc. Natl. Acad. Sci. USA *111*, 1772–1777.

Orekhov, V.Y., and Jaravine, V.A. (2011). Analysis of non-uniformly sampled spectra with multi-dimensional decomposition. Prog. Nucl. Magn. Reson. Spectrosc. *59*, 271–292.

Pellegrini, L., Burke, D.F., von Delft, F., Mulloy, B., and Blundell, T.L. (2000). Crystal structure of fibroblast growth factor receptor ectodomain bound to ligand and heparin. Nature *407*, 1029–1034.

Phillips, J.C., Braun, R., Wang, W., Gumbart, J., Tajkhorshid, E., Villa, E., Chipot, C., Skeel, R.D., Kalé, L., and Schulten, K. (2005). Scalable molecular dynamics with NAMD. J. Comput. Chem. *26*, 1781–1802.

Plotnikov, A.N., Schlessinger, J., Hubbard, S.R., and Mohammadi, M. (1999). Structural basis for FGF receptor dimerization and activation. Cell *98*, 641–650.

Ruch, C., Skiniotis, G., Steinmetz, M.O., Walz, T., and Ballmer-Hofer, K. (2007). Structure of a VEGF-VEGF receptor complex determined by electron microscopy. Nat. Struct. Mol. Biol. *14*, 249–250.

Schlessinger, J. (2003). Signal transduction. Autoinhibition control. Science *300*, 750–752.

Schubert, C., Schalk-Hihi, C., Struble, G.T., Ma, H.C., Petrounia, I.P., Brandt, B., Deckman, I.C., Patch, R.J., Player, M.R., Spurlino, J.C., and Springer, B.A. (2007). Crystal structure of the tyrosine kinase domain of colony-stimulating factor-1 receptor (cFMS) in complex with two inhibitors. J. Biol. Chem. *282*, 4094–4101.

Shalaby, F., Rossant, J., Yamaguchi, T.P., Gertsenstein, M., Wu, X.F., Breitman, M.L., and Schuh, A.C. (1995). Failure of blood-island formation and vasculogenesis in Flk-1-deficient mice. Nature *376*, 62–66.

Shalaby, F., Ho, J., Stanford, W.L., Fischer, K.D., Schuh, A.C., Schwartz, L., Bernstein, A., and Rossant, J. (1997). A requirement for Flk1 in primitive and definitive hematopoiesis and vasculogenesis. Cell *89*, 981–990.

Shen, Y., Delaglio, F., Cornilescu, G., and Bax, A. (2009). TALOS+: a hybrid method for predicting protein backbone torsion angles from NMR chemical shifts. J. Biomol. NMR *44*, 213–223.

Smith, S.O., Smith, C.S., and Bormann, B.J. (1996). Strong hydrogen bonding interactions involving a buried glutamic acid in the transmembrane sequence of the neu/erbB-2 receptor. Nat. Struct. Biol. *3*, 252–258.

Olsson, M.H.M., Soedergaard, C.R., Rostkowski, M., and Jensen, J. (2000). PROPKA3: Consistent Treatment of Internal and Surface Residues in Empirical pKa Predictions. J. Chem. Theory Comput. *7*, 525–537.

Stauber, D.J., DiGabriele, A.D., and Hendrickson, W.A. (2000). Structural interactions of fibroblast growth factor receptor with its ligands. Proc. Natl. Acad. Sci. USA *97*, 49–54.

Tao, R.H., and Maruyama, I.N. (2008). All EGF(ErbB) receptors have preformed homo- and heterodimeric structures in living cells. J. Cell Sci. *121*, 3207–3217.

Walter, M., Lucet, I.S., Patel, O., Broughton, S.E., Bamert, R., Williams, N.K., Fantino, E., Wilks, A.F., and Rossjohn, J. (2007). The 2.7 A crystal structure of the autoinhibited human c-Fms kinase domain. J. Mol. Biol. *367*, 839–847.

Webster, M.K., and Donoghue, D.J. (1996). Constitutive activation of fibroblast growth factor receptor 3 by the transmembrane domain point mutation found in achondroplasia. EMBO J. *15*, 520–527.

Yuzawa, S., Opatowsky, Y., Zhang, Z., Mandiyan, V., Lax, I., and Schlessinger, J. (2007). Structural basis for activation of the receptor tyrosine kinase KIT by stem cell factor. Cell *130*, 323–334.

Zhang, X., Gureasko, J., Shen, K., Cole, P.A., and Kuriyan, J. (2006). An allosteric mechanism for activation of the kinase domain of epidermal growth factor receptor. Cell *125*, 1137–1149.